Dalton Transactions

PAPER

View Article Online
View Journal | View Issue

Cite this: *Dalton Trans.*, 2014, **43**, 5823

Solvents and auxiliary ligands co-regulate three antiferromagnetic Co(II) MOFs based on a semi-rigid carboxylate ligand†

Lin Cui, Guo-Ping Yang, Wei-Ping Wu, Hui-Hui Miao, Qi-Zhen Shi and Yao-Yu Wang*

Received 27th November 2013,
Accepted 29th December 2013

DOI: 10.1039/c3dt53342e

www.rsc.org/dalton

By reacting an asymmetry semi-rigid Y-shaped/L-shaped linker H_3cpta (H_3cpta = 3-(4′-carboxyphenoxy)-phthalic acid) and $Co(CH_3COO)_2{\cdot}6H_2O$ under different N-donor ligands in different solvents, three new Co-based coordination polymers, $[Co_3(cpta)_2(bpe)_3(H_2O)_4]$ (**1**) $[Co(\mu_2\text{-}H_2O)(\mu_3\text{-}OH)(Hcpta)(bpe)(H_2O){\cdot}3(DMF)3(H_2O)]$ (**2**) and $[Co_3(cpta)_2(bpa)_4]$ (**3**) have been obtained. They exhibit trinodal topological nets/layer, based on Co^{2+} ions and Y-shaped/L-shaped carboxylate linkers. **1** and **3** present 3D frameworks with the point symbol $\{4{\cdot}10^2\}_2\{10^5{\cdot}12\}\{4{\cdot}8^5\}_2$ for **1** and $\{4{\cdot}8^2\}_2\{8^5{\cdot}9\}\{4{\cdot}6^7{\cdot}9^2\}_2$ for **3**. While, **2** exhibits a 2D layer with the point symbol $\{4{\cdot}6{\cdot}8\}\{4{\cdot}6^2{\cdot}8^3\}\{6^2{\cdot}8\}$. The magnetic studies indicate that all of the three complexes show antiferromagnetic exchanges transmitted through μ_3-carboxylate/μ_4-carboxylate bridges, μ_2-H_2O molecules and μ_3-OH ions between Co^{2+} ions, respectively. And the result of this research shows that the solvent and the secondary ligands could co-regulate coordination polymer with interesting properties, providing a constructive guidance when synthesizing versatile topologies with the same organic spacer but a different architecture.

Introduction

On account of the potential applications in molecule magnetism, ion exchange, catalysis, gas storage, nonlinear optics and luminescence, great interest has been focused on the rapidly expanding field of coordination polymers.[1] An effective strategy to obtain coordination polymers (CPs) with the functions mentioned above is the self-assembly method, in which the metal salts and the organic spacers such as carboxylates are mixed in a one-pot reaction. Nevertheless, there still exists a huge challenge in the self-assembly synthesis of CPs of how to predict the final structures of the compounds, because the reaction process might be influenced by a number of factors, such as temperature, solvent, metal–ligand ratio, counter ion, the nature of spacers, pH and even supramolecular interactions.[2] Although polycarboxylate ligands can bridge rigid metal clusters as nodes into CPs with structurally predictable frameworks, the variable coordination geometry of the carboxylate can easily link single metal ions in different modes into frameworks of unpredictable topologies.[3]

Recent research has shown that the so-called semirigid V-shaped multicarboxylate ligands with two aromatic rings bridged by a nonmetallic atom (C, O, S, or N atom) as central molecular framework are of great flexibility, which could be able to lead to metal complexes with diverse structures because of the free rotation of two benzene rings around the bridged nonmetallic atom. While, the symmetric semi-rigid V-shaped multidentate O-donor ligands with two of four carboxylic substituents attached at the symmetric positions of the semi-rigid V-shaped central molecular framework usually generate coordination polymers with discrete metal ions as node, leading to limitations in tuning the structure and functionality of coordination polymers (CPs).[4] Therefore, efforts have been started recently devoted to the construction of CPs using asymmetric semi-rigid V-shaped multidentate O-donor ligands with carboxylic substituents attached at asymmetric positions of the central V-shaped molecular framework, obtaining interesting frameworks with diverse structures and potential applications in the field of separation, magnetism, absorption, catalyst and sensors.[5] In contrast to the extensive studies of the CPs formed from symmetrical V-shaped organic ligands, asymmetrical semi-rigid V-shaped multi-dentate O-donor ligands with different numbers of carboxylic substituents at each benzene ring of the central molecular framework have been relatively less investigated.[6] Despite the isolation of

Key Laboratory of Synthetic and Natural Functional Molecule Chemistry of the Ministry of Education, Shaanxi Key Laboratory of Physico-Inorganic Chemistry, College of Chemistry and Materials Science, Northwest University, Xi'an, Shaanxi, P. R. China. E-mail: wyaoyu@nwu.edu.cn; Fax: (+86)-29-88303798

†Electronic supplementary information (ESI) available. CCDC 965948–965950 for compounds **1–3**. For ESI and crystallographic data in CIF or other electronic format see DOI: 10.1039/c3dt53342e

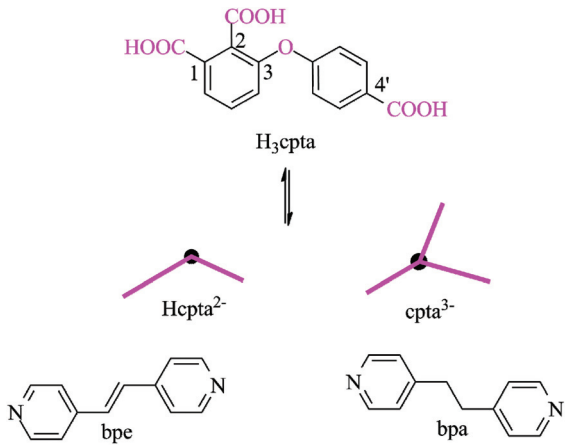

Scheme 1 Schematic molecular structures of H_3L and N-donor ligands.

interesting CPs comprising polymetallic clusters and nanotube subunits on the basis of a preliminary study employing mixed V-shaped asymmetric multicarboxylate and N-donor ligands reacting with transitional metal ions, it seems still significant to provide more novel organic–inorganic hybrid complexes with a different assembly principle towards further clarifying the relationship between the symmetry of V-shaped multidentate O-donor ligands and the structures of CPs under different solvents. Therefore, an asymmetry semi-rigid Y-shaped/L-shaped linker H_3cpta (H_3cpta = 3-(4′-carboxyphenoxy)phthalic acid) (Scheme 1) is used to construct frameworks with more versatile topologies.

In this work, two 3D CPs $[Co_3(cpta)_2(bpe)_3(H_2O)_4]$ (**1**) and $[Co_3(cpta)_2(bpa)_4]$ (**3**), one 2D layer coordination polymer $[Co(\mu_2\text{-}H_2O)(\mu_3\text{-}OH)(Hcpta)(bpe)(H_2O)\cdot 3(DMF)3(H_2O)]$ (**2**) have been synthesized under hydrothermal/solvothermal methods with different N-donor ligands-bpe, bpa (Scheme 1), which feature different trinodal topologies respectively. The Co(II)-based MOFs often exhibit excellent magnetic properties,[1] so the magnetic properties of the three CPs were investigated as well.

Experimental section

All chemicals and solvents are commercially available and were used as received without further purification. Elemental analyses for C, H, and N were determined with a Perkin-Elmer 2400C Elemental Analyzer at the Analysis and Test Research Center of Northwest University. Thermogravimetric analyses (TGA) were carried out in a nitrogen stream using a Netzsch TG209F3 equipment at a heating rate of 5 K min^{-1}. Powder X-ray diffraction (PXRD) data were recorded on a Bruker D8 ADVANCE X-ray powder diffractometer (Cu-Kα, λ = 1.5418 Å). Magnetic properties were tested on a Quantum Design MPMS-XL-7 SQUID magnetometer.

Synthesis of $[Co_3(cpta)_2(bpe)_3(H_2O)_4]$ (1)

A mixture of $Co(CH_3COO)_2\cdot 6H_2O$ (0.049 g, 0.20 mmol), H_3cpta (0.031 g, 0.10 mmol), bpe (0.037 g, 0.20 mmol) and NaOH (0.10 mL, 0.5 mol L^{-1}) in H_2O (10 mL) was stirred at room temperature for 30 min after which the mixture was transferred to a Teflon-lined stainless steel vessel (20 mL). The vessel was heated at 418 K for 72 h, then cooled to room temperature at a rate of 5 K h^{-1}, giving the pink block crystals of **1**, which were isolated by washing with H_2O, and drying in air. The yield $C_{66}H_{52}Co_3N_6O_{18}$ was *ca.* 67.9 mg (48.7%, based on the amount of H_3cpta). Anal. Calcd for: C, 56.87; H, 3.76; N, 6.03. Found: C, 55.30; H, 3.22; N, 6.33%. IR (KBr, cm^{-1}): 3433 m, 3218 m, 3039 w, 1604 vs, 1549 s, 1401 vs, 1211 w, 1064 m, 831 m, 763 m.

Synthesis of $[Co_2(\mu_2\text{-}H_2O)(\mu_3\text{-}OH)(Hcpta)(bpe)(H_2O)\cdot 3(DMF)\text{-}3(H_2O)]$ (2)

A mixture of $Co(CH_3COO)_2\cdot 6H_2O$ (0.049 g, 0.20 mmol), H_3cpta (0.031 g, 0.10 mmol), bpe (0.037 g, 0.20 mmol) and NaOH (0.10 mL, 0.5 mol L^{-1}) in DMF (2 mL) and H_2O (8 mL) was stirred at room temperature for 30 min after which the mixture was transferred to a Teflon-lined stainless steel vessel (20 mL). The vessel was heated at 418 K for 72 h, then cooled to room temperature at a rate of 5 K h^{-1}, giving the purple block crystals of **2**, which were isolated by washing with DMF, and drying in air. The yield $C_{36}H_{50}O_{16}N_5Co_2$ was *ca.* 45.4 mg (49.0%, based on the amount of H_3cpta). Anal. Calcd for: C, 46.66; H, 5.44; N, 7.56%. Found: C, 47.31; H, 5.30; N, 7.80. IR (KBr, cm^{-1}): 3440 m, 1598 vs, 1383 vs, 1248 w, 1101 m, 830 m, 763 m, 695 m.

Synthesis of $[Co_3(cpta)_2(bpa)_4]$ (3)

A mixture of $Co(CH_3COO)_2\cdot 6H_2O$ (0.049 g, 0.20 mmol), H_3cpta (0.031 g, 0.10 mmol), bpa (0.037 g, 0.20 mmol) and NaOH (0.10 mL, 0.5 mol L^{-1}) in H_2O (10 mL) was stirred at room temperature for 30 min after which the mixture was transferred to a Teflon-lined stainless steel vessel (20 mL). The vessel was heated at 418 K for 72 h, then cooled to room temperature at a rate of 5 K h^{-1}, giving the pink block crystals of 3, which were isolated by washing with H_2O, and drying in air. The yield of $C_{78}H_{62}Co_3N_8O_{14}$ was *ca.* 62.3 mg (41.2%, based on the amount of H_3cpta). Anal. Calcd for: C, 61.95; H, 4.13; N, 7.41. Found: C, 61.03; H, 4.27; N, 7.38%. IR (KBr, cm^{-1}): 3416 m, 3053 w, 1610 vs, 1561 s, 1432 vs, 1236 w, 1064 m, 812 m, 757 m.

X-Ray crystallography

The diffraction data were collected at 296(2) K for **1** and **2**, 293(2) K for **3** with a Bruker AXS Smart Apex diffractometer using ω rotation scans with a scan width of 0.3° and Mo-Kα radiation (λ = 0.71073 Å). The structures were solved by direct methods and refined by full-matrix least-squares refinements based on F^2 with the SHELXTL program.[7] All non-hydrogen atoms were refined anisotropically with the hydrogen atoms added to their geometrically ideal positions and refined isotropically. The guest molecules of **2** were highly disordered and could not be located in the structures. Thus the SQUEEZE routine of PLATON was applied to remove the contributions of scattering from the solvent molecules. The final formulae were

determined by combining single-crystal structures, elemental microanalyses and TGA data. Selected crystallographic data and structure refinement results are listed in Tables S1 and S2.† A semi-empirical absorption correction was applied using SADABS. The topological analysis and some diagrams were produced using the TOPOS program.[8]

Results and discussion

Synthesis

The formation of CPs is significantly influenced by the auxiliary ligands, solvent, pH value and so on. As shown in Scheme 1, the semi-rigid tricarboxylate ligand was chosen and used to assemble CPs **1–3** with the aid of the N-donor auxiliary ligands-bpe and bpa (Scheme 1). In the present research, **1** and **3** were prepared from the hydrothermal reaction between the tricarboxylate ligand (H_3cpta) and $Co(CH_3COO)_2{\cdot}6H_2O$ together with suitable N-donor ligands, however, Complex **2** was synthesized from the solvothermal reaction between H_3cpta and $Co(CH_3COO)_2{\cdot}6H_2O$ together with bpe. Introducing NaOH with a molar ratio of 2 : 1 to the ligand, the reaction between H_3cpta and $Co(CH_3COO)_2{\cdot}6H_2O$ without N-donor auxiliary ligands in different solution gave only some precipitates. However, when the N-donor ligands were introduced, excellent single crystals of the three complexes were obtained under suitable solvents, indicating the co-regulation effect of N-donor ligands and the solvents.

Structural description

Structure of $[Co_3(cpta)_2(bpe)_3(H_2O)_4]$ (1). Single-crystal X-ray analysis of **1** reveals that it crystallizes in the triclinic space group $P\bar{1}$. The asymmetric unit of **1** contains one and a half crystallographically independent Co^{2+} ions (Co1, 1/2 site occupancy; Co2, entire site occupancy), one fully deprotonated $cpta^{3-}$, three half bpe ligands and two terminal H_2O ligands. Each of the Co^{2+} atoms are octahedrally coordinated. The difference between the Co1 and Co2 is that Co1 is bound by two pyridyl N atoms from two crystallographically dependent bpe ligands, four carboxylate O atoms, two from carboxylates and two from H_2O ligands. However, Co2 is coordinated by two pyridyl atoms from two crystallographically independent bpe ligands, three oxygen atoms from two different $cpta^{3-}$ ligands and one oxygen atom from an aqua molecule (Fig. 1a). The Co–N and Co–O bond lengths are all within the normal ranges. Two Co2 atoms are connected by four $\eta^1{:}\eta^0{:}\eta^2{:}\mu_2$ *syn–syn–syn* carboxylate groups from two $cpta^{3-}$ to afford the $Co_2(O_2C)_4(H_2O)_2$ dimer (Fig. 1b) (Co···Co separation of 5.5302 Å). The dimer has a *C*2-symmetry with the axis traversing the center of the two Co2 atoms. A 4^4 two-dimensional (2D) network is formed by $cpta^{3-}$, Co2 atoms and bpe ligands (Fig. 1c) by ignoring the connections with Co1 and bpe ligands which eventually generate the three-dimensional (3D) framework of **1** (Fig. 1d).

Structure of $[Co(\mu_2\text{-}H_2O)(\mu_3\text{-}OH)(Hcpta)(bpe)(H_2O){\cdot}3(DMF){\cdot}3(H_2O)]$ (2). A single-crystal X-ray diffraction study of **2** reveals

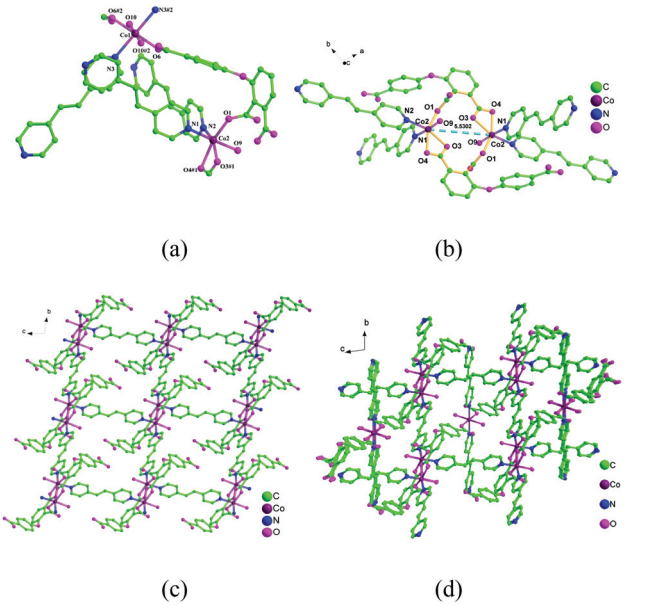

Fig. 1 (a) The coordination geometry for Co(II) atoms in **1** with the 30% probability level; all hydrogen atoms and water molecules have been omitted for clarity. (b) The coordination environment of Co2 dimer in **1**. (c) The 2D framework of Co2 by ignoring the connections with Co1 and bpe ligands. (d) The three-dimensional framework of **1**. [Symmetry codes: #1 = –*x*, 1 – *y*, 1 – *z*; #2 = 1 – *x*, –*y*, 2 – *z*].

a 2D layer that crystallizes in triclinic space group $P\bar{1}$. The asymmetric unit contains only one half of the chemical formula unit, which contains two Co^{2+} ions, one bpe molecule, one μ_2-H_2O molecule, one μ_3-OH anion, one-third of deprotonation $Hcpta^{2-}$ anion, one terminal and two lattice aqua molecules. Two crystallographically independent Co^{2+} ions with the same coordination environment bound by one μ_3-OH anion are observed in the structure. As shown in Fig. 2a, the Co1 atom is connected by two oxygen atoms from two different carboxylate groups, two oxygen atoms from two μ_3-OH anions, one oxygen atom from the μ_2-H_2O molecule and one nitrogen atom from the bpe ligand, giving an octahedral coordination geometry with considerable distortion. While, the Co2 atom resides in the same distorted octahedral environment, with the equatorial plane formed by three oxygen atoms from two carboxylate groups and one from the μ_3-OH anion bound with Co1, and the axial position occupied by one pyridyl nitrogen atom from the bpe ligand and one from the μ_2-H_2O group. Two Co1 and two Co2 are connected with each other *via* two μ_3-OH ions and two μ_2-H_2O molecules, and then form a $Co_4(\mu_3\text{-}OH)_2(\mu_2\text{-}H_2O)_2(O_2C)_4(H_2O)_2$ core by four μ_2-$\eta^1{:}\eta^1$-*syn*,*syn* carboxylate groups and two terminal aqua molecules (Fig. 2b, top) (Co···Co separation of 3.1864 Å and 3.5813 Å). The Co1–O(H)–Co2 angles are 100.5 and 120.9°, while the angles of Co1–O(H)–Co1 and Co1–O(H_2)–Co2 are 98.8 and 90.0°. Each core is symmetrically joined to adjacent cluster units by two μ_4-carboxylate bridges to form a zigzag metal–oxygen backbone running along the (1,1,1) direction. The adjoining metal–oxygen backbones are further extended to a 2D porous framework through the bpe spacer. The hydrogen bonds between the carboxylate and the

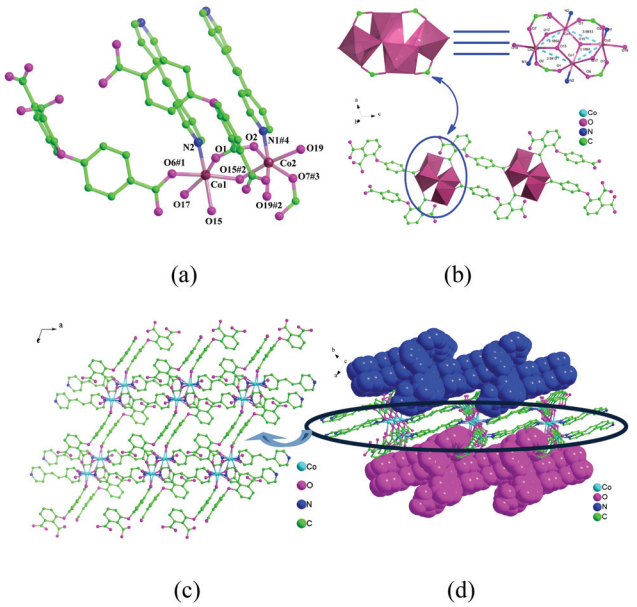

Fig. 2 (a) The coordination geometry for Co(II) atoms in **2** with the 30% probability level; all hydrogen atoms and water molecules have been omitted for clarity. (b) The coordination environment of $Co_4(\mu_3\text{-}OH)_2(\mu_2\text{-}H_2O)_2(O_2C)_4(H_2O)_2$ core in **2**. (c) The 2D porous framework of **2**. (d) The 3D supramolecular network of **2**. [Symmetry codes: #1 = $-x, -y, -z$; #2 = $-x, -y, 1-z$; #3 = $x, y, 1+z$; #4 = $1-x, 1-y, 1-z$].

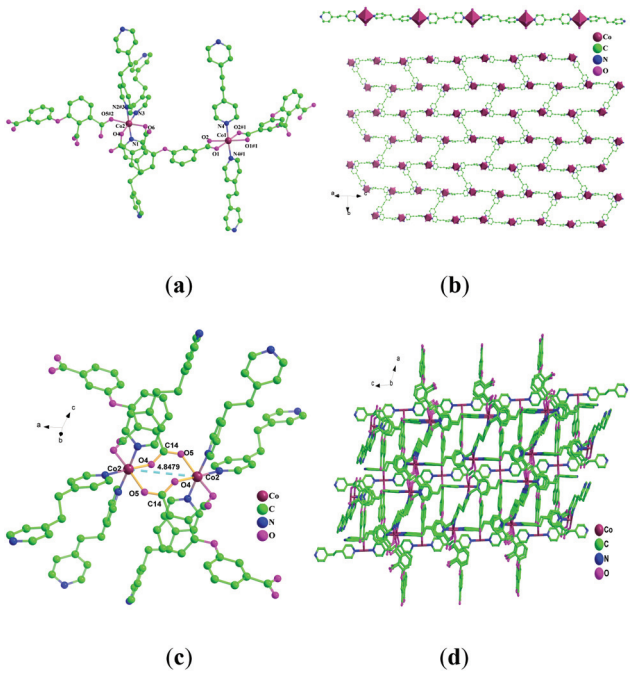

Fig. 3 (a) The coordination geometry for Co(II) atoms in **3** with the 30% probability level; all hydrogen atoms and water molecules have been omitted for clarity. (b) Co1 chain and Co2 layer formed by bpa. (c) The coordination environment of $[Co_2(O_2C\text{–})_2]$ unit in **3**. (d) The 3D network of **3**. [Symmetry codes: #1 = $2-x, y, 0.5-z$; #2 = $-x, 1-y, -z$; #3 = $x, 1-y, -0.5+z$].

lattice water molecules make the 2D adjacent layers connect with each other, generating a three-dimensional (3D) supramolecular network as illustrated in Fig. 2d.

Structure of $[Co_3(cpta)_2(bpa)_4]$ (3). Crystal **3** crystallizes in the monoclinic system, space group *P*2/*c*. Single-crystal structure analysis reveals that the asymmetric unit in **3** consists of two independent Co^{2+} cations, one of which is at half occupancy in the asu, the rest being generated by symmetry, one fully-deprotonated $cpta^{3-}$ anion, one and two halves of a bpa ligand. Of the two Co^{2+} centers, one Co1 is located in a distorted octahedral coordination geometry with the equatorial plane formed by four oxygen atoms from two carboxylate groups, and the axial position occupied by two nitrogen atoms from the bpa ligands. The other Co2 is located in a distorted octahedral geometry with three oxygen atoms from two different $cpta^{3-}$ ligands and one pyridyl atom from bpa ligand at basal positions, and two pyridyl atoms from two different bpa ligands at apical positions as shown in Fig. 3a. Co1 atoms are connected with each other by bpa ligands, forming 1D chains, while Co2 atoms form 2D layers (Fig. 3b). Two Co2 centers bridged by two carboxylate in *syn–anti* fashion form a $[Co_2(O_2C\text{–})_2]$ unit, with Co2···Co2 separation of 4.8479 Å (Fig. 3c). The Co1 chains and Co2 layers are further linked by μ_3-$cpta^{3-}$ ligands to generate 3D frameworks with Co–O bond distances ranging from 2.068 to 2.154 Å (Fig. 3d).

Topological analysis

Topologically, the $cpta^{3-}$ linkers in **1** and **3** and $Hcpta^{2-}$ linker in **2** all can be simplified as 3-connected nodes, respectively. Remarkably, the 4-connected Co^{2+} nodes in **1** and **3** display a significantly distorted octahedral environment, while the Co^{2+} centers show 4- or 5-connected. These nodes combine distorted Y-shaped $cpta^{3-}$ ligands to form a rarely trinodal (3,4,4)-connected net for **1** with the point symbol of $\{4\cdot10^2\}_2\{10^5\cdot12\}\text{-}\{4\cdot8^5\}_2$ (Fig. 4a) and (3,4,5)-connected net for **3** with the point symbol of $\{4\cdot8^2\}_2\{8^5\cdot9\}\{4\cdot6^7\cdot9^2\}_2$ (Fig. 4c). However, the Co1 and Co2 atoms in **2** display 3- and 4-connected nodes, these combine with the distorted L-shaped $Hcpta^{2-}$ ligands to form a trinodal (3,3,4)-connected layer with the point symbol of $\{4\cdot6\cdot8\}\{4\cdot6^2\cdot8^3\}\{6^2\cdot8\}$ (Fig. 4b).

Coordination modes

1 and **2** are synthesized with same initial reactants under different solvents. **1** is hydrothermally synthesized, however **2** is solvothermal with DMF–H_2O (v : v = 1 : 4). Compared to **1** and **2**, **3** is a hydrothermal reaction with H_3cpta, $Co(CH_3COO)_2\cdot6H_2O$ and bpa. Contrasting the coordination modes among the three CPs, carboxylic ligands show μ_3-bridged modes in **1** (Fig. 5a) and **3** (Fig. 5c), but the connection modes are different. The connection mode in **1** is $\mu_3\text{–}\eta^2\text{:}\eta^1\eta^0\text{:}\eta^1\eta^0$-*syn*,*syn*:*syn*:*syn* mode, and that of **3** is $\mu_3\text{–}\eta^2\text{:}\eta^0\eta^1\text{:}\eta^1\eta^1$-*syn*,*syn*:*anti*:*anti*,*syn*. However, the mode in **2** displays μ_4-bridged (Fig. 5b). The difference between **1** and **2** is the solvents used, and that of **1** and **3** is the N-donor ligands used. The co-regulation of secondary ligands and solvents might accelerate the synthesis of CPs with diverse properties.

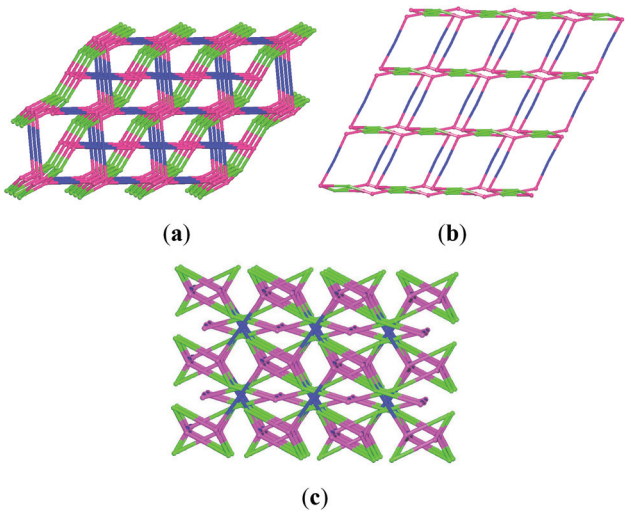

Fig. 4 (a) The (3,4,4)-connected net for **1**; (b) The (3,3,4)-connected layer for **2**; (c) The (3,4,5)-connected net for **3**. All of the purple balls represent Co^{2+} ions, while the blue ones for the bpa ligands, and green points represent the cpta ligands.

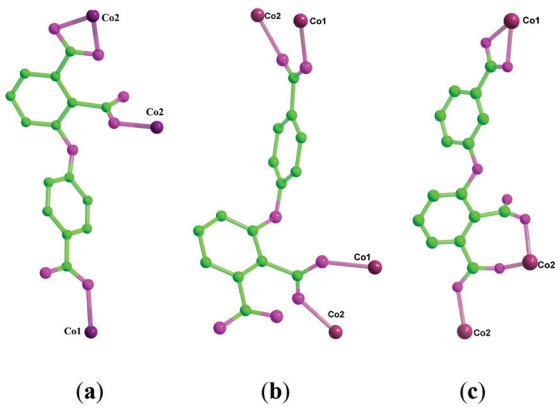

Fig. 5 (a) μ_3-bridged $cpta^{3-}$ in **1**; (b) μ_4-bridged $Hcpta^{2-}$ in **2**; (c) μ_3-bridged $cpta^{3-}$ in **3**. All hydrogen atoms have been omitted for clarity.

The effect of solvents used and secondary N-donor ligands

Despite the elucidation of the slight difference in the coordination modes in **1** and **3**, the intrinsic reason for the formation of diverse building units has not yet been clarified. It therefore appears necessary to further investigate the secondary N-donor ligands on the subunits. The configuration and flexibility of the secondary ligands play a key role in directing the related properties of the complexes. For **1**, rigid rod-like bpe was selected as an auxiliary ligand, and found to act as a connector to link adjacent 2D Co2-core layers and Co1 chains into a 3D structure. And for **3**, flexible bpa was selected as a secondary ligand, which adopts an *anti* conformation in the final network (Scheme 2), which might cause a similar coordination geometry of the center ions between **1** and **3**. However, the final structural topology of **3** is quite different to that of **1**, which might be due to the flexible secondary ligand used.

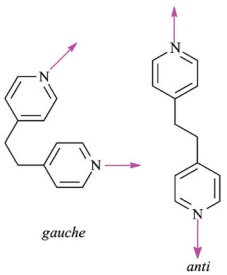

Scheme 2 Different conformations of bpa ligand.

Solvent effect is a vital subject in the construction of coordination polymers. Customarily, solvents may be broadly classified into two categories; polar and nonpolar, which can be characterized by their dielectric constants. And, it has been well noted that the coordination assemblies of specific reactants will be influenced by solvents used in reactions from both thermodynamic and kinetic aspects, which might yield diverse crystalline products. The structural differences between **1** and **2** may be attributed to the polarity and molecule size of the solvents. H_2O is a polar solvent, which has a larger dielectric constant and lower dipole moment, while, DMF has a lower dielectric constant and larger dipole moment, making it a nonpolar solvent (Table 1).[9] The factors mentioned above make water a good proton-donating agent, but DMF a poor proton-donating solvent. And the solvent-encircled H_3cpta molecules are coordinated to metal ions when they collide effectively. H_2O has a smaller van der Waals volume, which makes molecules collide more effectively, but the larger van der Waals volume of DMF makes the collisions more difficult. That is why **1** is a 3D structure and **2** is a 2D layer, although the same reactants were mixed initially.

PXRD and thermal analysis

To investigate the thermal stability of three compounds, thermal analyses have been carried out on a crystalline sample in a nitrogen atmosphere at a heating rate of 10 K min^{-1} (Fig. S1 in the ESI†). TGA of **1** exhibits a significant weight loss of 7.89% from room temperature to 170 °C (Fig. S1†), implying the release of all H_2O solvent molecules per formula unit (calc. 8.29%), followed by an abrupt weight loss followed immediately by the framework collapse. For **2**, the preliminary weight loss of 10.9% beginning at 240 °C to 290 °C corresponds to the removal of all H_2O ligands (calc. 11.6%), then followed by a plateau of stability from 290 to 310 °C, and then a weight loss

Table 1 Dielectric constant, dipole moment,[a] and van der Waals volume[b] for DMF and H_2O

Solvent	Dielectric constant	Dipole moment (*D*)	van der Waals volume (cm^3 mol^{-1})
DMF	38	3.82	47.67
H_2O	80	1.85	11.44

[a] Data taken from ref. 9*a*. [b] Data calculated using the formula in ref. 9*b*.

of 14.1% from 310 to 350 °C corresponds to the removal of all DMF ligands (calc. 13.7%), whereupon the rapid dissociation of $Hcpta^{2-}$ and bpe induces the framework decomposition. While the TGA of **3** shows a plateau from the beginning to 300 °C, exhibiting a good structural stability, and then followed by a rapid dissociation of the framework decomposition. The main framework of **3** is much more stable than those of **1** and **2**, which may be attributed to the flexible backbone of bpa ligand that make the network much denser. Matching the PXRD patterns of the bulk samples of **1**, **2** and **3** with their simulated patterns from the single-crystal structures, shows the phase purity of the as-synthesized products. The PXRD patterns of all the CPs were performed under Cu-Kα radiation (λ = 1.54056 Å). Because there is a strong X-ray fluorescent effect for the compounds containing Mn, Fe, Co, *etc.* the fluorescent background is difficult to eliminate (Fig. S2, S3 and S4†).

Magnetic property

The variable-temperature magnetic susceptibility (χ_M) of **1**, **2** and **3** were examined in a 1000 Oe field in the range 1.8–300 K. Because the bridging ligands H_3cpta, bpe and bpa are quite long in **1** and **3**, and thus the Co···Co distances are a little long too, the magnetic interaction transferred by these ligands should be very weak. The magnetic properties of **1** and **3** could be regarded as those of a Co2 dimer and a single metal ion anisotropy. Here, we only give the magnetic property of **1** as an example between **1** and **3**. As shown in Fig. 6, at 300 K, the $\chi_M T$ values of each framework for **1**, **2** and **3** are 10.13, 5.09 and 9.22 cm^3 K mol^{-1}, respectively. The values of **1** and **3** are much higher than the value for three magnetically isolated spin-only S = 3/2 Co^{2+} systems (5.625 cm^3 K mol^{-1}), which is as expected because of the significant orbit contribution of high-spin Co^{2+} ion in an octahedral coordination environment. For **1**, upon cooling, the $\chi_M T$ value declines monotonously and reaches 0.12 cm^3 K mol^{-1} at 1.8 K, indicating a significantly antiferromagnetic exchange between the magnetic centers in Co2 dimer. The antiferromagnetic interaction for Co^{2+}-carboxylate dimers is closely related to the Co···Co distances. In the Co2 unit of **1**, the magnetic coupling between Co2 dimer is transmitted through μ_1-$C_{benzene}$-$\mu_{1,3}$ carboxylate bridges. The long Co···Co distance of 5.5302 Å is responsible for the antiferromagnetic interaction in **1**, which is also found in other Co2-based complex with carboxylate bridges.[10] The experimental susceptibility data were fitted to the equation that considers the sum of $Co_2(O_2C)_4(H_2O)_2$ dimer and mononuclear Co^{2+} ion (eqn (1)), and it is reasonable to explain that (a) the mononuclear Co(N2O4) exhibits a Curie-type magnetic behavior (eqn (2)); (b) the magnetic exchange interaction between dimers through bridging ligands is quite weak and could be neglected in comparison with magnetic exchange in a dimer and (c) the magnetic exchange interaction between the dimer and the neighbour Co(N2O4) can also be ignored. Therefore, the observation that the $\chi_M T$ value decreases upon cooling probably means the existence of an antiferromagnetic exchange interaction in the dimer or single Co(N2O4) magnetic behavior (zero-field splitting and spin–orbital coupling, *etc.*). For the layer binuclear Co^{2+} dimer, if the spin–orbital coupling interaction is neglected the temperature dependence of the molar magnetic susceptibility could be expressed as eqn (4), where J represents the exchange constant between neighbouring Co(N2O4) groups in the $Co_2(O_2C)_4(H_2O)_2$ dimer and other symbols have their normal meanings.

$$\chi_M = \chi_{dimer} + \chi_{mononuclear} \quad (1)$$

$$\chi_{mononuclear} = \frac{C}{T} \quad (2)$$

$$C = \frac{Ng^2\beta^2}{4kT} S(S+1) \quad (3)$$

$$\chi_{dimer} = \frac{2Ng^2\beta^2}{kT} \times \frac{14e^{12J/KT} + 5e^{6J/KT} + e^{2J/KT}}{7e^{12J/KT} + 3e^{2J/KT} + 1} \quad (4)$$

But the molar magnetic susceptibility data of **1** could not be fitted according to the above magnetic exchange model, which is not surprising for the strong spin–orbital coupling interaction of high spin Co^{2+} ion. However, it is difficult to reproduce magnetic susceptibility as a function of temperature when combining magnetic coupling between the neighbouring Co^{2+} ions at the same time. In order to estimate the strength of the antiferromagnetic exchange interaction, the following simple phenomenological equation (eqn (5)) can be used, considering the strong spin–orbit coupling in **1**.[10]

$$\chi_M T = A\exp(-E_1/kT) + B\exp(-E_2/kT) \quad (5)$$

In this equation, $A + B$ equals to the Curie constant, E_1 and E_2 represent the activation energies corresponding to the spin–orbit coupling and the antiferromagnetic exchange interactions, respectively. The equation is in good agreement with the experimental data (Fig. 6). The best fitting result is $A + B$ = 11.25 cm^3 K mol^{-1}, E_1/k = 3.7017 K, and $-E_2/k$ = −31.41 K ($R = \sum[(\chi_M T)_{obs} - (\chi_M T)_{calc}]^2/\sum[(\chi_M T)_{obs}]^2$ = 0.008). The obtained value of $A + B$ is very close to that from the Curie–Weiss law equation (11.99 cm^3 K mol^{-1}, Fig. S5†) and E_1/k has no significant difference from those given in the literature for the effect of spin–orbit coupling and antiferromagnetic interaction.[10]

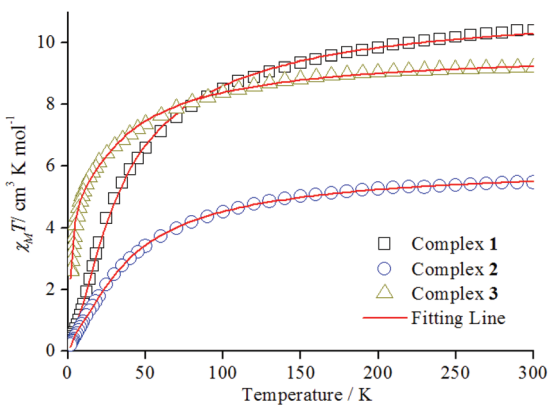

Fig. 6 Temperature dependence of $\chi_M T$ for **1** **2** and **3** (open symbols and red lines represent experimental data and fits).

The value of $-E_2/k$ (−31.41 K) indicates the dominant antiferromagnetic coupling between Co(II) ions as analyzed from the structure of the dimer. For **2**, the best fitting result is $A + B = 6.10$ cm^3 K mol^{-1}, $E_1/k = 4.20$ K, and $-E_2/k = -37.66$ K ($R = \sum[(\chi_M T)_{obs} - (\chi_M T)_{calc}]^2/\sum[(\chi_M T)_{obs}]^2 = 1.11 \times 10^{-2}$) and the obtained value of $A + B$ is very close to that from the Curie–Weiss law equation (6.63 cm^3 K mol^{-1}, Fig. S6†). While for **3**, the best fitting results are $A + B = 9.15$ cm^3 K mol^{-1}, $E_1/k = 41.35$ K, and $-E_2/k = -1.78$ K ($R = \sum[(\chi_M T)_{obs} - (\chi_M T)_{calc}]^2/\sum[(\chi_M T)_{obs}]^2 = 8.02 \times 10^{-2}$). As for **1** and **2**, the obtained value of $A + B$ is very close to that from the Curie–Weiss law equation (9.45 cm^3 K mol^{-1}, Fig. S7†).

The $\chi_M T$ values at room temperature between **1** and **3** are almost the same as each other, which is due to the same coordination orientation of bpe and *anti*-bpa. But the $\chi_M T$ values at 1.8 K are very different, which is due to the flexible backbone of the *anti*-bpa, making a closer distance with the Co ions between the Co2 dimer (**2**, 4.8479 Å; **3**, 5.5302 Å). Comparing the $\chi_M T$ values at room temperature between **1** and **2**, the value of **1** is almost two times that of **2**, which means a strong spin–orbit coupling. This phenomenon is due to the solvent used.

Conclusions

In conclusion, three new magnetic MOFs with semi-rigid carboxylate ligand (3-(4′-carboxyphenoxy)phthalic acid) and different N-donor auxiliary ligands have been synthesized under different solvent conditions. Complexes **1** and **3** show the same μ_3-carboxylate bridges with different linkage types although the same solvent is used, which might be due to different N-donor ligands. However, **1** and **2** are synthesized with the same reactants and the structural investigation shows different carboxylate bridges because of the solvents used. All of the complexes show antiferromagnetic interaction between Co^{2+} ions. In summary, the research demonstrates a co-regulation effect of auxiliary ligands and the reacting solvents, giving a guiding reference when synthesizing MOFs with attractive properties. And the further investigation of H_3cpta will be studied in our laboratory.

Acknowledgements

This work is supported by State Key Program of National Natural Science of China (no. 20931005), Key Research Planning Program of National Natural Science Foundation of China (Grant no. 91022004), National Natural Science Foundation of China (Grant 21371142 and 21201139), Natural Science Foundation of Shaanxi Province (Grant 2013JQ2016), Science Research Plan Projects of Shaanxi Provincial Educational Department (Grant 12JK0605).

References

1 (*a*) P. Dechambenoit and J. R. Long, *Chem. Soc. Rev.*, 2011, **40**, 3249–3265; (*b*) H. L. Jiang and Q. Xu, *Chem. Commun.*, 2011, **47**, 3351–3370; (*c*) *Metal Organic Frameworks: Applications from Catalysis to Gas Storage*, ed. D. Farrusseng, Wiley, Weinheim, 2011; (*d*) Z. J. Lin, T. F. Liu, X. L. Zhao and R. Cao, *Cryst. Growth Des.*, 2011, **11**, 4284–4287; (*e*) L. Hou, W. J. Shi, Y. Y. Wang, Y. Guo, C. Jin and Q. Z. Shi, *Chem. Commun.*, 2011, **47**, 5464–5466; (*f*) Z. Z. Lu, R. Zhang, Y. Z. Li, Z. J. Guo and H. G. Zheng, *J. Am. Chem. Soc.*, 2011, **133**, 4172–4177; (*g*) I. Eryazici, O. K. Farha, O. C. Compton, C. Stern, J. T. Hupp and S. T. Nguyen, *Dalton Trans.*, 2011, **40**, 9189–9193; (*h*) M. V. Lucky, S. Sivakumar, M. L. P. Reddy, A. K. Paul and S. Natarajan, *Cryst. Growth Des.*, 2011, **11**, 857–864; (*i*) S. R. Batten, S. M. Neville and D. R. Turner, *Coordination Polymers: Design, Analysis and Application*, Springer, New York, 2010; (*j*) F. Nouar, J. Eckert, J. F. Eubank, P. Forster and M. Eddaoudi, *J. Am. Chem. Soc.*, 2009, **131**, 2864–2870; (*k*) H. X. Deng, S. Grunder, K. E. Cordova, C. Valente, H. Furukawa, M. Hmadeh, F. Gándara, A. C. Whalley, Z. Liu, S. Asahina, H. Kazumori, M. O'Keeffe, O. Terasaki, J. F. Stoddart and O. M. Yaghi, *Science*, 2012, **336**, 1018–1023; (*l*) D. S. Li, J. Zhao, Y. P. Wu, B. Liu, L. Bai, K. Zou and M. Du, *Inorg. Chem.*, 2013, 8091–8098; (*m*) D. S. Li, F. Fu, J. Zhao, Y. P. Wu, M. Du, K. Zou, W. W. Dong and Y. Y. Wang, *Dalton Trans.*, 2010, **39**, 11522–11525.

2 (*a*) X. M. Zhang, *Coord. Chem. Rev.*, 2005, **249**, 1201–1219; (*b*) B. Moulton and M. J. Zaworoto, *Chem. Rev.*, 2001, **101**, 1629–1658.

3 (*a*) H. Li, M. Eddaoudi, M. O'Keeffe and O. M. Yaghi, *Nature*, 1999, **402**, 276–279; (*b*) G. Ferey, C. Serre, F. Millange, J. Dutour, S. Surble and I. Margiolaki, *Science*, 2005, **309**, 2040–2042; (*c*) D. S. Li, Y. P. Wu, J. Zhao, J. Zhang and J. Y. Lu, *Coord. Chem. Rev.*, 2014, **261**, 1–27.

4 (*a*) M. Eddaoudi, J. Kim, N. Rosi, D. Vodak, J. Wachter, M. O'Keefe and O. M. Yaghi, *Science*, 2002, **295**, 469–472; (*b*) C. Serre, F. Millange, J. Marrot and G. Férey, *Chem. Mater.*, 2002, **14**, 2409–2415; (*c*) H. Chun, H. Jung, G. Koo, H. Jeong and D. K. Kim, *Inorg. Chem.*, 2008, **47**, 5355–5359; (*d*) L. Xu, E. Y. Choi and Y. U. Kwon, *Inorg. Chem.*, 2007, **46**, 10670–10680; (*e*) J. W. Ye, J. Wang, J. Y. Zhang, P. Zhang and Y. Wang, *CrystEngComm*, 2007, **9**, 515–523; (*f*) D. Bradshaw, T. J. Prior, E. Cussen, J. B. Claridge and M. J. Rosseinsky, *J. Am. Chem. Soc.*, 2004, **126**, 6106–6114; (*g*) Z. Lin, D. S. Wragg, J. E. Warren and R. E. Morris, *J. Am. Chem. Soc.*, 2007, **129**, 10334–10335; (*h*) D. R. Xiao, E. B. Wang, H. Y. An, Y. G. Li, Z. M. Su and C. Y. Sun, *Chem.–Eur. J.*, 2006, **12**, 6528–6541.

5 (*a*) X. L. Wang, C. Qin, E. B. Wang, Y. G. Li, Z. M. Su, L. Xu and L. Carlucci, *Angew. Chem., Int. Ed.*, 2005, **44**, 5824–5827; (*b*) P. Mahata, G. Madras and S. Natarajan, *J. Phys. Chem. B*, 2006, **110**, 13759–13768; (*c*) S. L. Li, Y. Q. Lan, J. F. Ma, J. Yang, G. H. Wei, L. P. Zhang and Z. M. Su, *Cryst.*

Growth Des., 2008, **8**, 1610–1616; (*d*) Y. Q. Lan, S. L. Li, K. Z. Shao, X. L. Wang, D. Y. Du, Z. M. Su and D. J. Wang, *Cryst. Growth Des.*, 2009, **9**, 1353–1360; (*e*) X. L. Chen, B. Zhang, H. M. Hu, F. Fu, X. L. Wu, T. Qin, M. L. Yang, G. L. Xue and J. W. Wang, *Cryst. Growth Des.*, 2008, **8**, 3706–3870; (*f*) Q. Chu, G. X. Liu, Y. Q. Huang, X. F. Wang and W. Y. Sun, *Dalton Trans.*, 2007, 4302–4311.

6 (*a*) H. Wang, D. Zhang, D. Sun, Y. Chen, L. F. Zhang, L. Tian, J. Jiang and Z. H. Ni, *Cryst. Growth Des.*, 2009, **9**, 5273–5282; (*b*) H. Wang, D. Zhang, D. Sun, Y. Chen, K. Wang, Z. H. Ni, L. Tian and J. Jiang, *CrystEngComm*, 2010, **12**, 1096–1102; (*c*) S. Q. Zhang, F. L. Jiang, M. Y. Wu, J. Ma, Y. Bu and M. C. Hong, *Cryst. Growth Des.*, 2012, **12**, 1452–1463.

7 G. M. Sheldrick, *SHELXL, version 6.12*, Bruker Analytical Instrumentation, Madison, WI, 2000.

8 V. A. Blatov, A. P. Shevchenko and V. N. J. Serezhkin, *Appl. Crystallogr.*, 2000, **33**, 1193.

9 (*a*) C. Y. Niu, X. F. Zheng, X. S. Wan and C. H. Kou, *Cryst. Growth Des.*, 2011, **11**, 2874–2888; (*b*) L.-F. Ma, L.-Y. Wang, M. Du and S. R. Batten, *Inorg. Chem.*, 2010, **49**, 365–367.

10 (*a*) J. M. Rueff, N. Masciocchi, P. Rabu, A. Sironi and A. Skoulios, *Eur. J. Inorg. Chem.*, 2001, 2843–2848; (*b*) X. Y. Wang and S. C. Sevov, *Inorg. Chem.*, 2008, **47**, 1037–1043; (*c*) L. L. Liang, S. B. Ren, J. Wang, J. Zhang, Y. Z. Li, H. B. Du and X. Z. You, *CrystEngComm*, 2010, **12**, 2669–2671.